nature materials

LETTERS

PUBLISHED ONLINE: 2 FEBRUARY 2015 | DOI: 10.1038/NMAT4205

Light-emitting diodes by band-structure engineering in van der Waals heterostructures

F. Withers[1], O. Del Pozo-Zamudio[2], A. Mishchenko[1], A. P. Rooney[3], A. Gholinia[3], K. Watanabe[4], T. Taniguchi[4], S. J. Haigh[3], A. K. Geim[5], A. I. Tartakovskii[2] and K. S. Novoselov[1]*

The advent of graphene and related 2D materials[1,2] has recently led to a new technology: heterostructures based on these atomically thin crystals[3]. The paradigm proved itself extremely versatile and led to rapid demonstration of tunnelling diodes with negative differential resistance[4], tunnelling transistors[5], photovoltaic devices[6,7] and so on. Here, we take the complexity and functionality of such van der Waals heterostructures to the next level by introducing quantum wells (QWs) engineered with one atomic plane precision. We describe light-emitting diodes (LEDs) made by stacking metallic graphene, insulating hexagonal boron nitride and various semiconducting monolayers into complex but carefully designed sequences. Our first devices already exhibit an extrinsic quantum efficiency of nearly 10% and the emission can be tuned over a wide range of frequencies by appropriately choosing and combining 2D semiconductors (monolayers of transition metal dichalcogenides). By preparing the heterostructures on elastic and transparent substrates, we show that they can also provide the basis for flexible and semi-transparent electronics. The range of functionalities for the demonstrated heterostructures is expected to grow further on increasing the number of available 2D crystals and improving their electronic quality.

The class of two-dimensional (2D) atomic crystals[1], which started with graphene[2], now includes a large variety of materials. However, even larger diversity can be achieved if one starts to combine several such crystals in van der Waals heterostructures[3,8]. Most attractive and powerful is the idea of band-structure engineering, where by combining several different 2D crystals one can create a designer potential landscape for electrons to live in. Rendering the band structure with atomic precision allows tunnel barriers, QWs and other structures, based on the broad choice of 2D materials.

Such band-structure engineering has previously been exploited to create LEDs and lasers based on semiconductor heterostructures grown by molecular beam epitaxy[9]. Here we demonstrate that using graphene as a transparent conductive layer, hexagonal boron nitride (hBN) as tunnel barriers and different transition metal dichalcogenides[1,10] (TMDCs) as the materials for QWs, we can create efficient LEDs (Fig. 1f). In our devices, electrons and holes are injected into a layer of TMDC from the two graphene electrodes. As a result of the long lifetime of the quasiparticles in the QWs (determined by the height and thickness of the neighbouring hBN barriers), electrons and holes recombine, emitting a photon. The emission wavelength can be fine-tuned by the appropriate selection of TMDC and quantum efficiency (QE) can be enhanced by using multiple QWs (MQWs).

We chose TMDCs because of wide choice of such materials and the fact that monolayers of many TMDCs are direct-bandgap semiconductors[11–15]. Until now, electroluminescence (EL) in TMDC devices has been reported only for lateral monolayer devices and attributed to thermally assisted processes arising from impact ionization across a Schottky barrier[16] and formation of p–n junctions[15,17,18]. The use of vertical heterostructures allows us to improve the performance of LEDs in many respects: reduced contact resistance, higher current densities allowing brighter LEDs, luminescence from the whole device area (Fig. 1e,f) and wider choice of TMDCs and their combinations allowed in designing such heterostructures. The same technology can be extended to create other QW-based devices such as indirect excitonic devices[19], LEDs based on several different QWs and lasers.

Figure 1 schematically shows the architecture of single-quantum-well (SQW) and MQW structures along with optical images of a typical device (Fig. 1e). We used a peel/lift van der Waals technique[20] to produce our devices (see Methods and Supplementary Information for further details on device fabrication). In total we measured more than a dozen of such QW structures comprising single and multiple layers of TMDC flakes from different materials: MoS_2, WS_2 and WSe_2. The yield was 100% with every device showing strong EL that remains unchanged after months of periodic measurements, which demonstrates the robustness of the technology and materials involved.

Cross-sectional bright-field scanning transmission electron microscope (STEM) images of our SQW and MQW devices demonstrate that the heterostructures are atomically flat and free from interlayer contamination[21] (Fig. 1b,d). The large atomic numbers for TMDCs allow the semiconductor crystals to be clearly identified owing to strong electron-beam scattering (dark contrast observed in Fig. 1b,d). Other layers were identified by energy-dispersive X-ray spectroscopy. The large intensity variation partially obscures the lattice contrast between adjacent layers but, despite this, the hBN lattice fringes can clearly be seen in Fig. 1b,d. The different contrast of the four MoS_2 monolayers in the MQW of Fig. 1d is attributed to their different crystallographic orientations (confirmed by rotating the sample around the heterostructure's vertical direction, which changes the relative intensity of different layers).

For brevity we concentrate on current–voltage (I–V) characteristics, photoluminescence (PL) and EL spectra from

[1]School of Physics and Astronomy, University of Manchester, Oxford Road, Manchester M13 9PL, UK. [2]Department of Physics and Astronomy, University of Sheffield, Sheffield S3 7RH, UK. [3]School of Materials, University of Manchester, Oxford Road, Manchester M13 9PL, UK. [4]National Institute for Materials Science, 1-1 Namiki, Tsukuba 305-0044, Japan. [5]Manchester Centre for Mesoscience and Nanotechnology, University of Manchester, Oxford Road, Manchester M13 9PL, UK. *e-mail: kostya@manchester.ac.uk

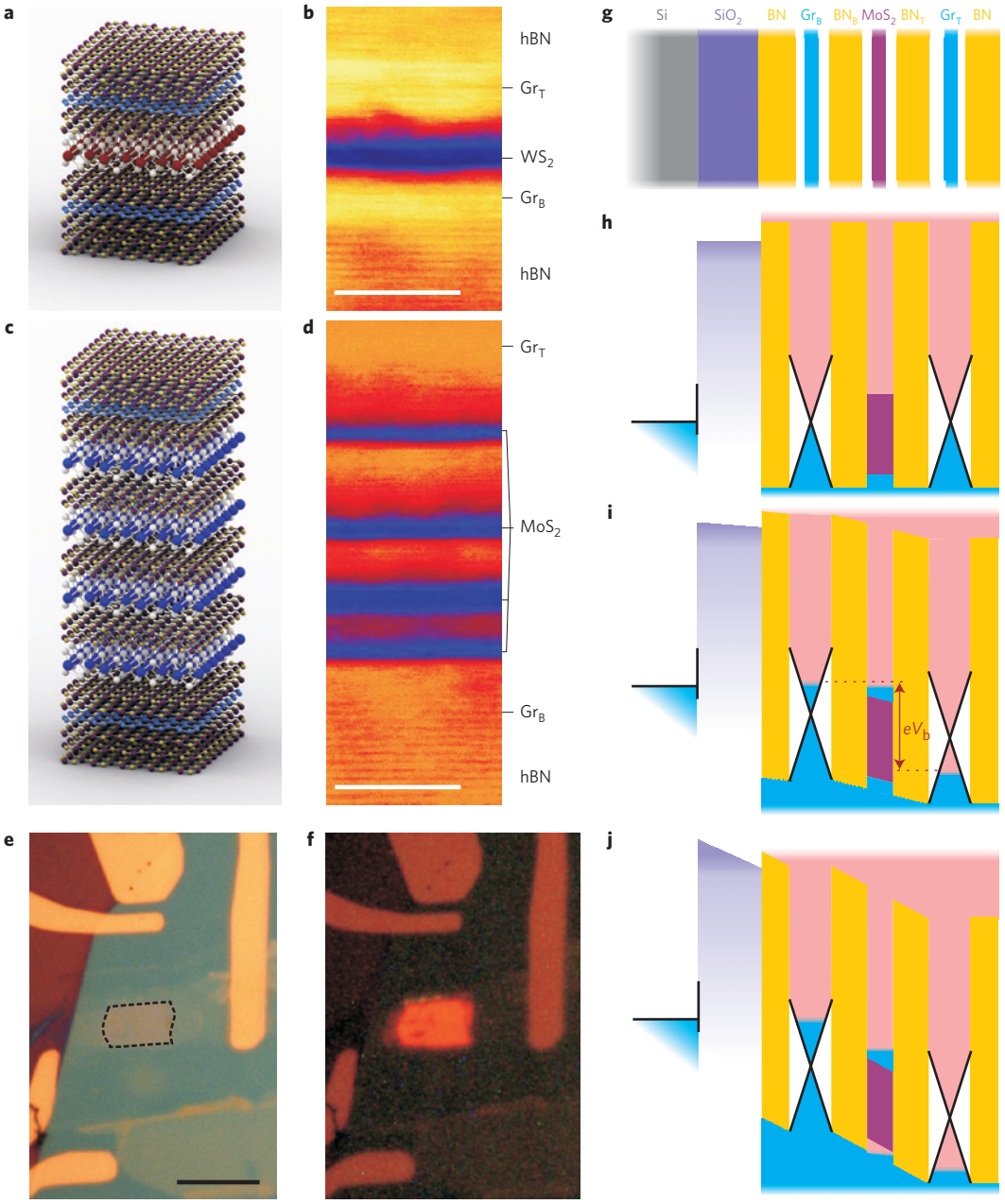

Figure 1 | Heterostructure devices with a SQW and MQWs. a, Schematic of the SQW heterostructure hBN/Gr_B/2hBN/WS_2/2hBN/Gr_T/hBN. **b**, Cross-sectional bright-field STEM image of the type of heterostructure presented in **a**. Scale bar, 5 nm. **c**,**d**, Schematic and STEM image of the MQW heterostructure hBN/Gr_B/2hBN/MoS_2/2hBN/MoS_2/2hBN/MoS_2/2hBN/MoS_2/2hBN/Gr_T/hBN. The number of hBN layers between MoS_2 QWs in **d** varies. Scale bar, 5 nm. **e**, Optical image of an operational device (hBN/Gr_B/3hBN/MoS_2/3hBN/Gr_T/hBN). The dashed curve outlines the heterostructure area. Scale bar, 10 μm. **f**, Optical image of EL from the same device. $V_b = 2.5$ V, $T = 300$ K. 2hBN and 3hBN stand for bi- and trilayer hBN, respectively. **g**, Schematic of our heterostructure consisting of Si/SiO_2/hBN/Gr_B/3hBN/MoS_2/3hBN/Gr_T/hBN. **h**–**j**, Band diagrams for the case of zero applied bias (**h**), intermediate applied bias (**i**) and high bias (**j**) for the heterostructure presented in **g**.

symmetric devices based on MoS_2 (Fig. 2a–c). Devices based on WS_2 and devices with asymmetric barriers are considered in the Supplementary Information.

At low V_b, the PL in Fig. 2a is dominated by the neutral A exciton, X^0, peak[12] at 1.93 eV. We attribute the two weaker and broader peaks at 1.87 and 1.79 eV to bound excitons[22,23]. At a certain V_b, the PL spectrum changes abruptly with another peak emerging at 1.90 eV. This transition is correlated with an increase in the differential conductivity (Fig. 2a). We explain this transition as being due to the fact that at this voltage the Fermi level in the bottom graphene electrode (Gr_B) rises above the conduction band in MoS_2, allowing injection of electrons into the QW (Fig. 1i). This allows us to determine the band alignment between the Dirac point in graphene and the bottom of the conductance band in MoS_2: the offset equals half of the bias voltage at which the tunnelling through states in the conductance band of MoS_2 is first observed. To take into account the effects of possible variance in the thickness of hBN barriers and small intrinsic doping of graphene, we average the onset of tunnelling through MoS_2 for positive and negative bias voltages (Fig. 2a), which yields the offset to be ~0.5 eV—in agreement with theoretical prediction[24,25]. Note, that the alignment of graphene's Dirac point with respect

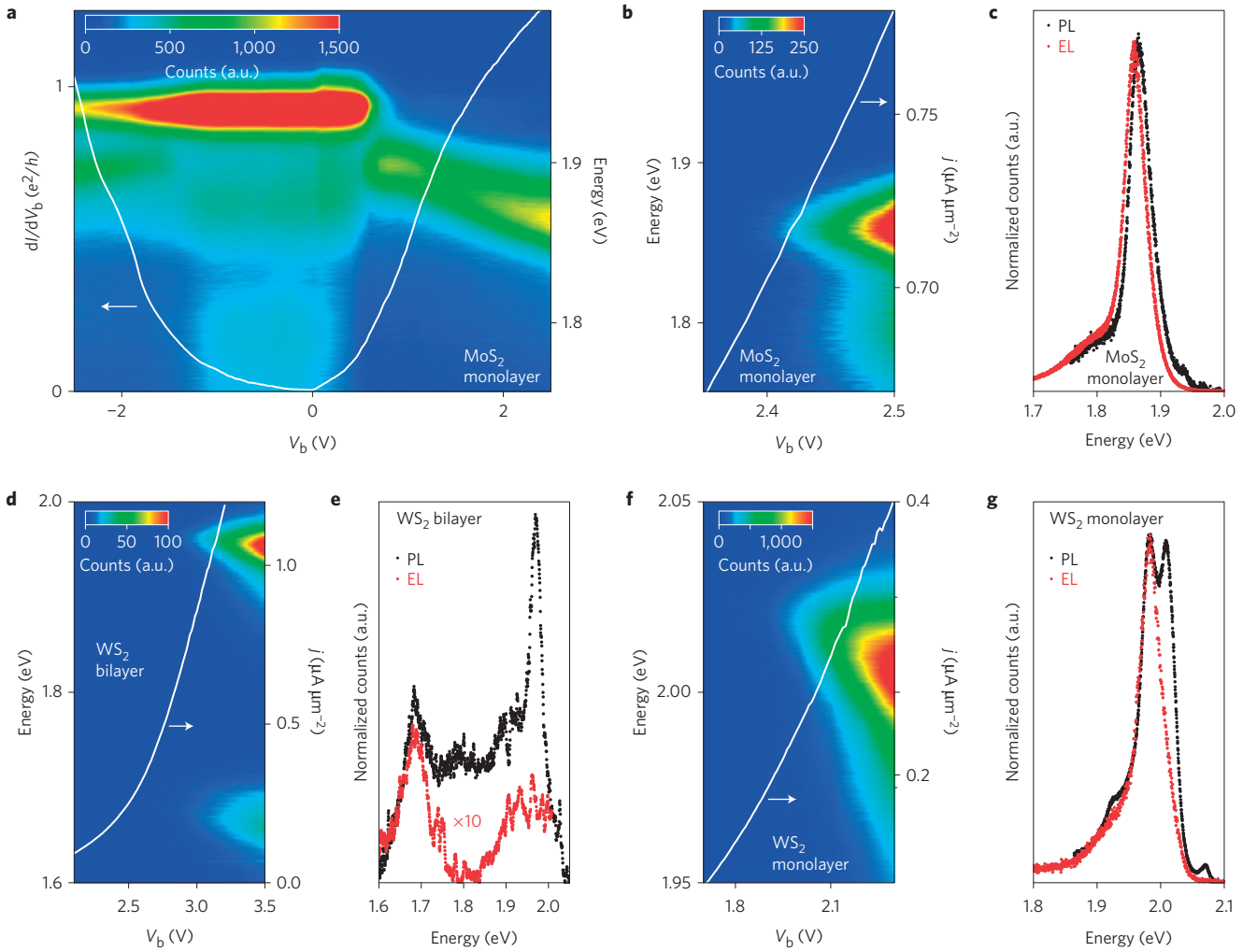

Figure 2 | Optical and transport characterization of our SQW devices, $T = 7$ K. a, Colour map of the PL spectra as a function of V_b for a MoS_2-based SQW. The white curve is the dI/dV_b of the device. Excitation energy $E_L = 2.33$ eV. **b**, EL spectra as a function of V_b for the same device as in **a**. White curve: its j–V_b characteristic (j is the current density). **c**, Comparison of the PL and EL spectra for the same device. As PL and EL occur in the same spectral range, we measured them separately. **d**–**g**, The same as in **b**,**c** but for the bilayer (**d**,**e**) and monolayer (**f**,**g**) WS_2 QWs. The PL curves were taken at $V_b = 2.4$ V (**c**), 2.5 V (**e**) and 2 V (**g**); the EL curves were taken at $V_b = 2.5$ V (**c**), 2.5 V (**e**) and 2.3 V (**g**).

to the valence band in hBN has been measured in tunnelling experiments previously[5,26,27].

Injection of electrons into the conduction band of MoS_2 leads not only to an increase in tunnelling conductivity but, also, to accumulation of electrons in MoS_2 and results in formation of negatively charged excitons[12], X^-. The X^- peak is positioned at a lower energy compared with the X^0 peak owing to the binding energy, E_B, of X^-. In the case of MoS_2 we estimate E_B as ≈36 meV near the onset of X^-. As the bias increases, the energy of the X^- peak shifts to lower values, which can be attributed either to the Stark effect or to the increase in the Fermi energy in MoS_2 (ref. 12).

In contrast to PL, EL starts only at V_b above a certain threshold (Fig. 2b). We associate such behaviour with the Fermi level of the top graphene (Gr_T) being brought below the edge of the valence band so that holes can be injected into MoS_2 from Gr_T (in addition to electrons already injected from Gr_B) as sketched in Fig. 1j. This creates conditions for exciton formation inside the QW and their radiative recombination. We find that the EL frequency is close to that of PL at $V_b \approx 2.4$ V (Fig. 2a–c), which allows us to attribute the EL to radiative recombination of X^-. Qualitatively similar behaviour is observed for WS_2 QWs (Fig. 2d–g).

An important parameter for any light-emission device is the QE defined as $\eta = N2e/I$ (here e is the electron charge, and N is the number of the emitted photons). For SQWs we obtain quantum efficiencies of ~1%—this value by itself is ten times larger than that of planar p–n diodes[15,17,18] and 100 times larger than EL from Schottky barrier devices[16]. Our rough estimations show that the external QE (EQE) for PL is lower than that for EL. Relatively low EQE found in PL indicates that the crystal quality itself requires improvement and that even higher EQE in EL may then be achieved[28].

To enhance QE even further, we have employed multiple QWs stacked in series, which increases the overall thickness of the tunnel barrier and enhances the probability for injected carriers to recombine radiatively. Figure 3 shows results for one of such MQW structures with three MoS_2 QWs (layer sequence: Si/SiO_2/hBN/Gr_B/3hBN/MoS_2/3hBN/MoS_2/3hBN/MoS_2/3hBN/Gr_T/hBN) and another MQW with four asymmetric MoS_2 QWs (Fig. 1c,d) is described in the Supplementary Information. The current increases with V_b in a step-like manner, which is attributed to sequential switching of the tunnelling current through individual MoS_2 QWs. PL for the MQW device is qualitatively similar to that of SQW devices but the X^0 peak is replaced with a X^- peak at $V_b = 0.4$ V (Fig. 3c). The X^0 peak reappears again at

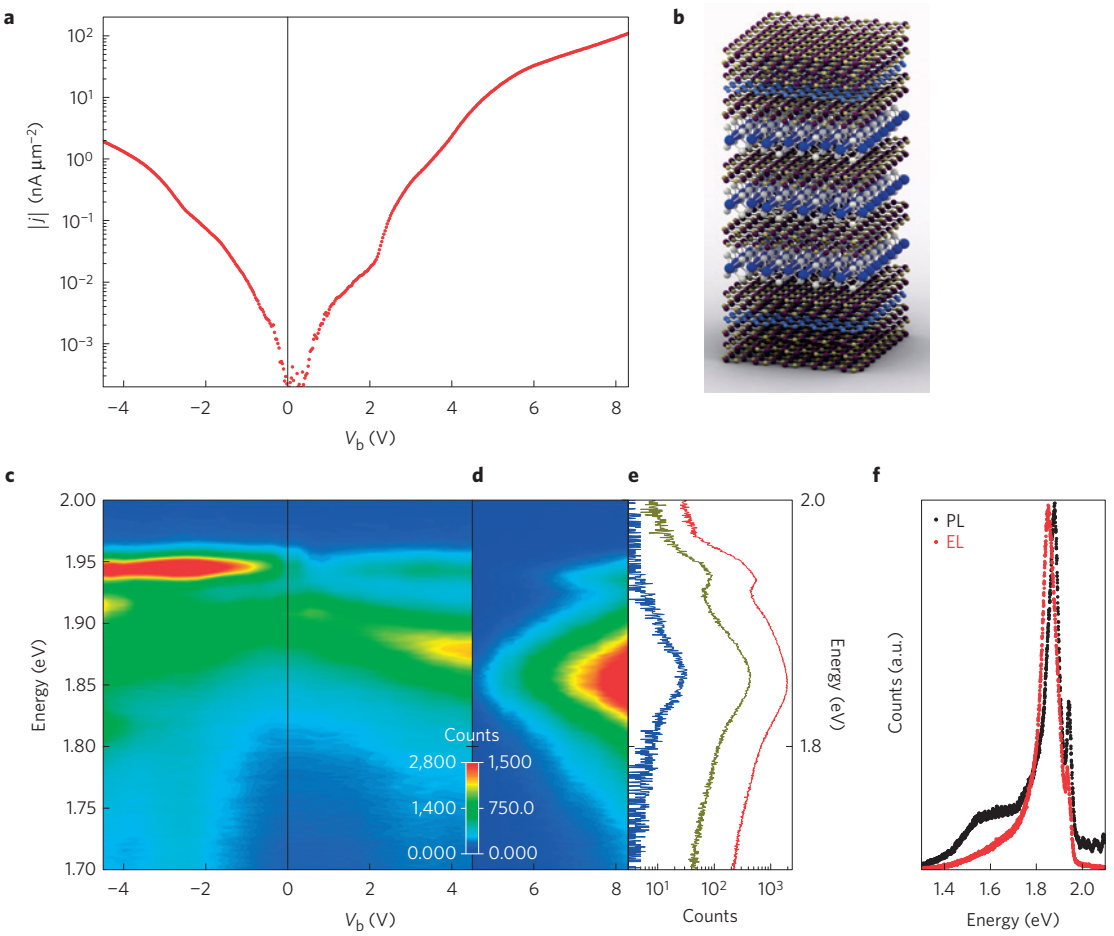

Figure 3 | Optical and transport characteristics of MQW devices, $T = 7$ K. a, Modulus of the current density through a triple QW structure based on MoS_2. **b**, Its schematic structure. **c**,**d**, Maps of PL and EL spectra for this device. $E_L = 2.33$ eV. **e**, Individual EL spectra plotted on a logarithmic scale show the onset of EL at 1.8 nA μm^{-2} (blue curve). Olive and red: $j = 18$ and 130 nA μm^{-2}, respectively. **f**, Comparison of the EL (taken at $V_b = 8.3$ V) and PL (taken at $V_b = 4.5$ V) spectra.

$V_b > 1.2$ V. This can be explained by charge redistribution between different QWs. The EL first becomes observable at $V_b > 3.9$ V and j of 1.8 nA μm^{-2} (Fig. 3d,e). This current density is nearly 2 orders of magnitude smaller than the threshold current required to see EL in similar SQWs. Importantly, the increased probability of radiative recombination is reflected in higher QE, reaching values of ~8.4% (for the device with quadruple QW, 6% for triple). This high QE is comparable to the efficiencies of the best modern-day organic LEDs (ref. 29).

The described technology of making designer MQWs offers the possibility of combining various semiconductor QWs in one device. Figure 4a–c describes an LED made from WSe_2 and MoS_2 QWs: Si/SiO_2/hBN/Gr_B/3hBN/WSe_2/3hBN/MoS_2/3hBN/Gr_T/hBN. EL and PL occur here in the low-E part of the spectra and can be associated with excitons and charged excitons in WSe_2. However, in comparison with SQW devices, the combinational device in Fig. 4 exhibits intensities more than an order of magnitude stronger for both PL and EL, yielding ~5% QE. We associate this with charge transfer between the MoS_2 and WSe_2 layers such that electron–hole pairs are created in both layers but transfer to and recombine in the material with the smaller bandgap[30]. Such a process is expected to depend strongly on band alignment, which is controlled by bias and gate voltages. This explains the complex, asymmetric V_b dependence of PL and EL in Fig. 4.

Generally, the fine control over the tunnelling barriers allows a reduction in the number of electrons and holes escaping from the quantum well, thus enhancing EQE. EQE generally demonstrates a peak at T around 50–150 K, depending on the material. Depending on the particular structure we found that typical values of EQE for MoS_2- and WS_2-based devices at room T are close or a factor of 2–3 lower than those at low T (Fig. 4d).

Finally, we note that because our typical stacks are only 10–40 atoms thick, they are flexible and bendable and, accordingly, can be used for making flexible and semi-transparent devices. To prove this concept experimentally, we have fabricated a MoS_2 SQW on a thin PET (polyethylene terephthalate) film (Fig. 4e,f). The device shows PL and EL very similar to those in Fig. 2a–c. We also tested the device's performance under uniaxial strain of up to 1% (using bending) and found no changes in the EL spectrum (Fig. 4g).

In summary, we have demonstrated band-structure engineering with one atomic layer precision by creating QW heterostructures from various 2D crystals including several TMDCs, hBN and graphene. Our LEDs based on a single QW already exhibit QE of above 1% and line widths down to 18 meV, despite the relatively poor quality of available TMDC layers. This EQE can be improved significantly by using multiple QWs. Consisting of 3 to 4 QWs, these devices show EQEs up to 8.4%. Combining different 2D semiconductor materials allows fine-tuning of the emission spectra and also an enhanced EL with a quantum yield of 5%. These values of QE are comparable to modern-day organic LED lighting and the concept is compatible with the popular idea of flexible and transparent electronics. The rapid progress in technology

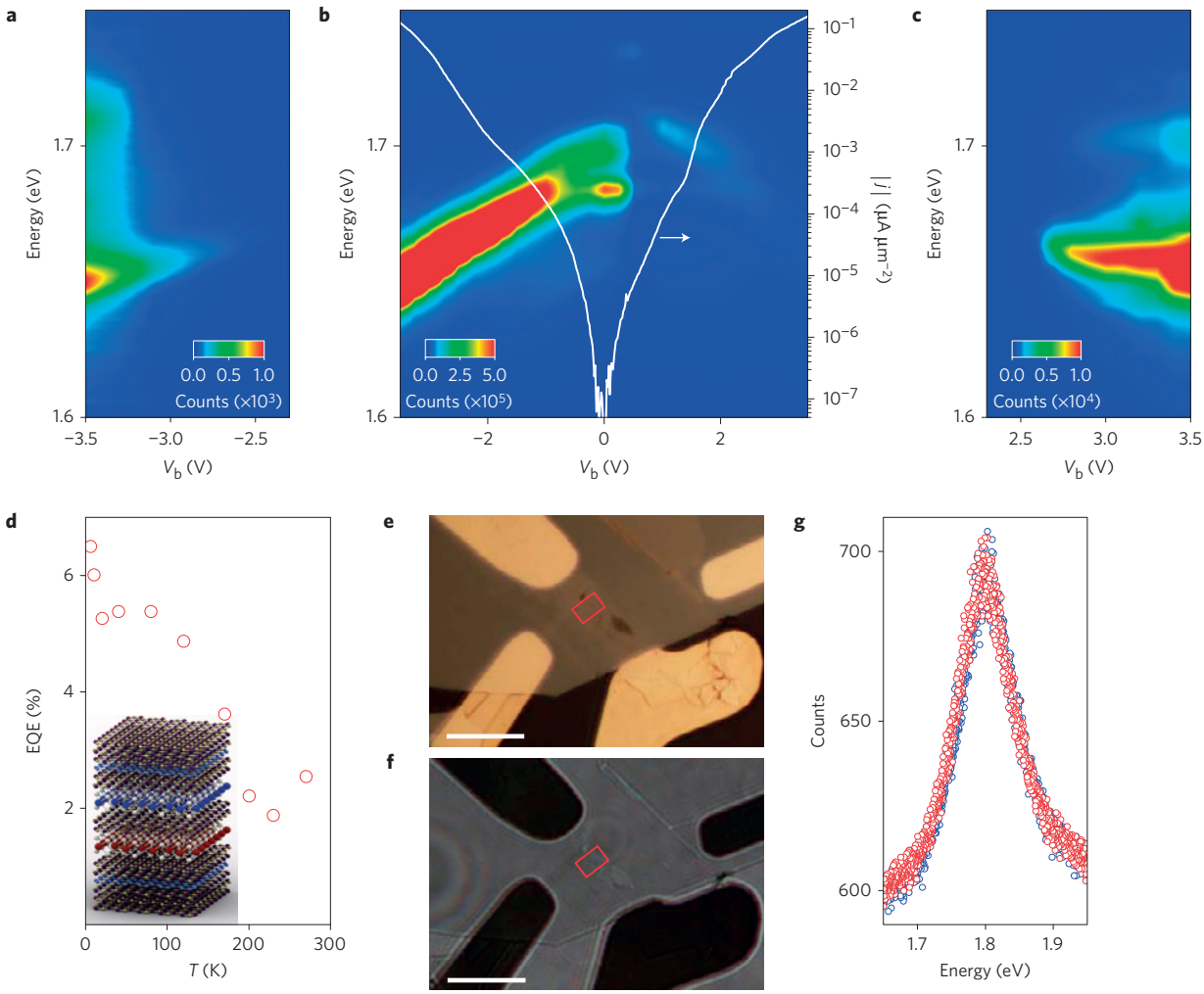

Figure 4 | Devices combining different QW materials and on flexible substrates. a–c, EL at negative (**a**) and positive (**c**) bias voltages for the device with two QWs made from MoS_2 and WSe_2 schematically shown in the inset in **d**. Its PL bias dependence is shown in **b**, for laser excitation $E_L = 2.33$ eV, $T = 7$ K. White curve: $|j|$–V_b characteristics of the device. **d**, Temperature dependence of EQE for a device with two QWs made from MoS_2 and WSe_2. Inset: schematic representation of a device with two QWs produced from different materials. **e**, Optical micrograph taken in reflection mode of a SQW (MoS_2) device on PET. **f**, Optical micrograph of the same device as in **e** taken in transmission mode. For **e**,**f** the area of the stack is marked by red rectangles; scale bars are 10 μm. **g**, EL spectra for the device in **e**,**f** at zero (blue dots) and 1% (red dots) strain. $V_b = -2.3$ V, $I = -40$ μA at room T.

of chemical vapour deposition growth will allow scaling up of production of such heterostructures.

Methods

Sample fabrication. Flakes of graphene, hBN and TMDCs are prepared by micromechanical exfoliation of bulk crystals. Single- or few-layer flakes are identified by optical contrast and Raman spectroscopy. Heterostructures are assembled using the dry peel/lift method described in detail in the Supplementary Methods. Electrical contacts to the top and bottom graphene electrodes are patterned using electron-beam lithography followed by evaporation of 5 nm Cr/60 nm Au.

Electrical and optical measurements. Samples are mounted within a liquid helium flow cryostat with a base temperature of $T = 6$ K. Electrical injection is performed using a Keithley 2400 source meter. To measure PL the samples were excited with a continuous wave 532 nm laser, focused to a spot size of ~1 μm through a ×50 objective (NA = 0.55) at a power less than required to modify the spectral line shape. The signal was collected and analysed using a single spectrometer and a nitrogen cooled CCD (charge-coupled device).

Scanning transmission electron microscopy. STEM imaging was carried out using a Titan G2 probe-side aberration-corrected STEM operating at 200 kV and equipped with a high-efficiency ChemiSTEM energy-dispersive X-ray detector. The convergence angle was 19 mrad and the third-order spherical aberration was set to zero (±5 μm). The multilayer structures were oriented along the ⟨hkl0⟩ crystallographic direction by taking advantage of the Kikuchi bands of the silicon substrate. (See Supplementary Information and ref. 21 for more detailed description.)

Received 19 November 2014; accepted 23 December 2014; published online 2 February 2015

References

1. Novoselov, K. S. *et al.* Two-dimensional atomic crystals. *Proc. Natl Acad. Sci. USA* **102,** 10451–10453 (2005).
2. Novoselov, K. S. *et al.* Electric field effect in atomically thin carbon films. *Science* **306,** 666–669 (2004).
3. Geim, A. K. & Grigorieva, I. V. Van der Waals heterostructures. *Nature* **499,** 419–425 (2013).
4. Britnell, L. *et al.* Resonant tunnelling and negative differential conductance in graphene transistors. *Nature Commun.* **4,** 1794 (2013).
5. Britnell, L. *et al.* Field-effect tunneling transistor based on vertical graphene heterostructures. *Science* **335,** 947–950 (2012).
6. Britnell, L. *et al.* Strong light–matter interactions in heterostructures of atomically thin films. *Science* **340,** 1311–1314 (2013).
7. Yu, W. J. *et al.* Highly efficient gate-tunable photocurrent generation in vertical heterostructures of layered materials. *Nature Nanotech.* **8,** 952–958 (2013).

8. Novoselov, K. S. Nobel lecture: Graphene: Materials in the flatland. *Rev. Mod. Phys.* **83,** 837–849 (2011).
9. Yao, Y., Hoffman, A. J. & Gmachl, C. F. Mid-infrared quantum cascade lasers. *Nature Photon.* **6,** 432–439 (2012).
10. Wang, Q. H., Kalantar-Zadeh, K., Kis, A., Coleman, J. N. & Strano, M. S. Electronics and optoelectronics of two-dimensional transition metal dichalcogenides. *Nature Nanotech.* **7,** 699–712 (2012).
11. Mak, K. F., Lee, C., Hone, J., Shan, J. & Heinz, T. F. Atomically thin MoS_2: A new direct-gap semiconductor. *Phys. Rev. Lett.* **105,** 136805 (2010).
12. Mak, K. F. *et al.* Tightly bound trions in monolayer MoS_2. *Nature Mater.* **12,** 207–211 (2013).
13. Xiao, D., Liu, G-B., Feng, W., Xu, X. & Yao, W. Coupled spin and valley physics in monolayers of MoS_2 and other group-VI dichalcogenides. *Phys. Rev. Lett.* **108,** 196802 (2012).
14. Ross, J. S. *et al.* Electrical control of neutral and charged excitons in a monolayer semiconductor. *Nature Commun.* **4,** 1474 (2013).
15. Ross, J. S. *et al.* Electrically tunable excitonic light-emitting diodes based on monolayer WSe_2 p–n junctions. *Nature Nanotech.* **9,** 268–272 (2014).
16. Sundaram, R. S. *et al.* Electroluminescence in single layer MoS_2. *Nano Lett.* **13,** 1416–1421 (2013).
17. Pospischil, A., Furchi, M. M. & Mueller, T. Solar-energy conversion and light emission in an atomic monolayer p–n diode. *Nature Nanotech.* **9,** 257–261 (2014).
18. Baugher, B. W. H., Churchill, H. O. H., Yang, Y. & Jarillo-Herrero, P. Optoelectronic devices based on electrically tunable p–n diodes in a monolayer dichalcogenide. *Nature Nanotech.* **9,** 262–267 (2014).
19. Rivera, P. *et al.* Observation of long-lived interlayer excitons in monolayer $MoSe_2$–WSe_2 heterostructures. Preprint at http://arXiv.org/abs/1403.4985 (2014).
20. Wang, L. *et al.* One-dimensional electrical contact to a two-dimensional material. *Science* **342,** 614–617 (2013).
21. Haigh, S. J. *et al.* Cross-sectional imaging of individual layers and buried interfaces of graphene-based heterostructures and superlattices. *Nature Mater.* **11,** 764–767 (2012).
22. Tongay, S. *et al.* Defects activated photoluminescence in two-dimensional semiconductors: Interplay between bound, charged, and free excitons. *Sci. Rep.* **3,** 2657 (2013).
23. Sercombe, D. *et al.* Optical investigation of the natural electron doping in thin MoS_2 films deposited on dielectric substrates. *Sci. Rep.* **3,** 3489 (2013).
24. Kang, J., Tongay, S., Zhou, J., Li, J. B. & Wu, J. Q. Band offsets and heterostructures of two-dimensional semiconductors. *Appl. Phys. Lett.* **102,** 012111 (2013).
25. Sachs, B. *et al.* Doping mechanisms in graphene-MoS_2 hybrids. *Appl. Phys. Lett.* **103,** 251607 (2013).
26. Lee, G. H. *et al.* Electron tunneling through atomically flat and ultrathin hexagonal boron nitride. *Appl. Phys. Lett.* **99,** 243114 (2011).
27. Britnell, L. *et al.* Electron tunneling through ultrathin boron nitride crystalline barriers. *Nano Lett.* **12,** 1707–1710 (2012).
28. Gutierrez, H. R. *et al.* Extraordinary room-temperature photoluminescence in triangular WS_2 monolayers. *Nano Lett.* **13,** 3447–3454 (2013).
29. Reineke, S. *et al.* White organic light-emitting diodes with fluorescent tube efficiency. *Nature* **459,** 234–238 (2009).
30. Lee, C. H. *et al.* Atomically thin p–n junctions with van der Waals heterointerfaces. *Nature Nanotech.* **9,** 676–681 (2014).

Acknowledgements

This work was supported by The Royal Society, Royal Academy of Engineering, US Army, European Science Foundation (ESF) under the EUROCORES Programme EuroGRAPHENE (GOSPEL), European Research Council, EC-FET European Graphene Flagship, Engineering and Physical Sciences Research Council (UK), the Leverhulme Trust (UK), US Office of Naval Research, US Defence Threat Reduction Agency, US Air Force Office of Scientific Research, FP7 ITN S^3NANO, SEP-Mexico and CONACYT.

Author contributions

F.W. produced experimental devices, led the experimental part of the project, analysed experimental data, participated in discussions, contributed to writing the manuscript; O.D.P-Z. measured device characteristics, participated in discussions, analysed experimental data; A.M. measured transport properties of the devices, participated in discussions; A.P.R. and A.G. produced samples for TEM study, analysed TEM results, participated in discussions; K.W. and T.T. grew high-quality hBN, participated in discussions; S.J.H. analysed TEM results, participated in discussions; A.K.G. analysed experimental data, participated in discussions, contributed to writing the manuscript; A.I.T. analysed experimental data, participated in discussions, contributed to writing the manuscript; K.S.N. initiated the project, analysed experimental data, participated in discussions, contributed to writing the manuscript.

Additional information

Supplementary information is available in the online version of the paper. Reprints and permissions information is available online at www.nature.com/reprints. Correspondence and requests for materials should be addressed to K.S.N.

Competing financial interests

The authors declare no competing financial interests.